Physical and Geometrical Modeling for
Image-Based Recovery of Left Ventricular Deformation

James Duncan, Ph.D.[†,*], Pengcheng Shi, Ph.D.[†], Todd Constable, Ph.D.[†], and Albert Sinusas, M.D.[‡]

Departments of [†]Diagnostic Radiology, [*]Electrical Engineering,

and [‡]Section of Cardiology

Yale University

P.O.Box 208042

New Haven, CT 06520

Please send correspondence to:

James S. Duncan, Ph.D.

Department of Diagnostic Radiology

Yale University

333 Cedar Street

New Haven, CT 06520

Abstract

Information about left ventricular (LV) mechanical performance is of critical importance in understanding the etiology of ischemic heart disease. Regional measurements derived from non–invasive imaging to assist in assessing this performance have been in use for decades, and certain parameters derived from these measurements often are useful clinically, as they correlate to some extent with gross physiological hypotheses. However, relatively little work has been done to date to carefully understand the relationship of regional myocardial injury to the local mechanical performance of the heart as derived from image data acquired non-invasively for a particular patient in 3 spatial dimensions over time. This paper describes efforts to take advantage of recent developments in 3D non-invasive imaging and biomechanical modeling to design an integrated computational platform capable of assembling a variety of displacement and velocity data derived from each image frame to deform a volumetric model representation of a portion of the myocardium. A brief description of both the reasoning behind this strategy is put forth, as well as an overview of the approach and some initial results are described.

Introduction

For several decades, researchers and practitioners in cardiology and cardiac radiology have been interested in deriving measures of regional left ventricular function from non-invasive (and even invasive) images [23, 42]. These measures have primarily come in the form of regional ejection fraction, regional shape change, and regional wall motion. It is our observation that in general these measures are trying to extract local descriptors of the pumping efficiency of each sector of the heart, which relates primarily to the mechanical performance of that portion of the myocardium. Furthermore, it is noted that the primary parameters in each case that are recorded from these image-derived measures are each related to radial changes in the heart wall, i.e. absolute position changes and/or thickness changes.

As noted in the clinical cardiology literature [36], the relative change in thickness, or thickening, seems to be the most important in terms of a quantitative indicator of the health of a section of the LV. It is critical to note that this image-derived information is fundamentally related to concepts from the field of continuum mechanics of deformable solids. This relative change in thickness is essentially equivalent to the mean value of the radial strain of this deformable solid, although if there is shearing the orientation of an initially radial vector will change. Furthermore, radial strain is only one component of a three-dimensional strain tensor that can more completely characterize the deformation of this object.

A primary goal of image analysis is often to recover quantitative information from noisy or otherwise corrupted image data. Often models are employed to help guide this recovery process, with the goal being to use real data to guide recovery when possible, but use the model as a smart interpolator in regions where the data are noisy, less reliable, or non-existent. Often these models are based on very mundane or simple strategies of simply maintaining smoothness everywhere. Rarely do we have the chance to invoke models that can truly attempt to describe the actual physical situation. In the recovery of cardiac LV performance, we have that rare opportunity, and due to the efforts of Hunter, McCulloch [20, 24] and others, there are even some previous efforts aimed at putting elegant models in touch with real live data.

This paper briefly reviews the use of computational models of the mechanics of the heart as applied to the problem of guiding the recovery of information about a particular heart from 3D diagnostic images. We are particularly interested in computationally accessible ideas which are suitable for integrating with the image-derived approaches. Certainly, however, one could also view these same strategies as a way of extracting data from images that can be used to help form better models of the LV structure that is being studied. We particularly focus on the problem of trying to recover information about the deformation of the LV everywhere in a finite-sized transaxial portion of the myocardium, i.e. both at the bounding surfaces of the LV as well as transmurally.

Overview on Image–Derived Measurement of Strain

Alternatives to Imaging. First, to motivate the goal stated in the Introduction, it is appropriate to note that there has been a variety of work in the cardiac physiology literature attempting to quantitatively measure transmural myocardial strain. Several noteworthy efforts in particular have used sonomicrometers ([13] and [11]) and arrays of implanted markers (see, for example, [16, 26, 42]). While accepted as being accurate, a key point about these techniques is that only a fairly sparse number of specific sites on the LV can measured, due to the difficulty in implanting the sonomicrometers and the markers. It would be quite difficult to measure a large number of sites simultaneously. Also, it is possible that these implanted devices can alter myocardial perfusion and function, although there is little published evidence of this. While many of these measurements are performed in animals, we note that some interesting measurements of strain using markers have been produced even in humans [21]. Finally, we also note that some researchers have looked at measuring *in vivo* strain using attached strain gauges [9] (as noted in [3]), although little has been pursued along these lines. See [43] for a very nice review of regional strain measurements in intact heart.

Non-invasive, Imaging- Based Strain Measurement. In addition to earlier work on coronary strain analysis from angiograms [47], work has been performed regarding the measurement of LV point-wise displacement using MR tagging as well as shape-based tracking of bounding surface displacements in recent years. Also, MR phase contrast techniques have been used to derive instantaneous velocity measurements. Each of these image data have been used separately to derive local LV strain measurements. While much of the focus here has been on the use of Magnetic Resonance Image (MRI) data (and this will be the primary image data utilized in the work described in this paper), it should be noted that via the shape-based tracking idea, measures can also be estimated from other 3D modalities with decent spatial resolution, e.g. 3D ultrasound and cine-CT. We note finally that there has been considerable effort within the medical image analysis and computer vision communities aimed at trying to correspond

and then map one surface into another, which is an important underlying aspect of many strain measurement approaches.

3D Deformation Analysis From MR Tagging. In this approach, grid lines at certain positions can be generated at one point in the cardiac cycle and their deformation tracked over a portion of the cycle, primarily using gated acquisition techniques. The development of the grid tagging approach to the measurement of myocardial strain has been vigorously pursued by two groups in particular, at the University of Pennsylvania [2] and Johns Hopkins University[49], who are the original developers of the tagging ideas. Much of these groups' current efforts are focused on how to create dense fields of measurements in 3D by putting together several orthogonal tagging grid acquisitions. Their approaches certainly show promise but have the following current limitations: i.) it's difficult to track the tags over the complete LV cycle due to decay of the tags with time, and ii.) it's still quite difficult to obtain acquisitions and assemble the detected tags into a robust 3D analysis/display with spatial resolution under 1cm in any direction. Both of these problems are being aggressively pursued by the two primary groups mentioned above, as well at a few other institutions, including somewhat within our own group ([1]). Regarding recent efforts pertaining to i.), [48] and [15] have created segmentation models to aid in the tag tracking process. Tag decay remains a fundamental issue, however, that is often solved by performing a second acquisition (a re-tagging) somewhere later in the cardiac cycle. Problem ii.) above is perhaps the most challenging one for MR tagging researchers. In order to obtain data pertaining to deformation in 3D, tag data must be acquired in two orthogonal views- typically short axis and long axis [3]. The same tissue elements are not tagged in each of the two views, and thus the deformation in each view must be seen as partial data that contributes to an overall scheme aimed at estimating the complete 3D deformation. This issue, plus the fact that the grid spacing is often quite far apart (on the order of 7mm spacing and 2-5mm thick tags for the SPAMM tagging done by Axel, et al. [46] and even further apart at the epicardium due to the radial tagging done by the Hopkins group [49]), is evidence that in most tagging schemes there is actually a rather sparse set of displacement estimates available based

on actual data, and some form of interpolation must be used to create a dense displacement field from which strain (or in fact any 3D map of motion and/or function) can be computed. A variety of approaches have been designed to attack this interpolation/estimation problem, with each approach making certain assumptions. Several of the most interesting ideas are the use of finite element model [46], the use of locally deformable superquadrics [31], and the use of stochastic models and statistical estimation techniques [8].

In [46], the authors fit a finite element grid to the corresponded tag grid displacements in order to interpolate between the sparse actual data points. The grid itself has a fairly small number of nodes however, and results in a fairly gross interpolation, although the errors computed in their simulations are reasonable. The goal in this work has been to compute the *mid*-ventricular strain present in the LV, and the paper includes a smooth surface visualization of the interpolated strains. This effort is related to our proposed approach here, although the key difference is in the motivation and the use of the finite element model. In [46], a finite element model is constructed as a geometrical representation of the left ventricle, and is used for fitting the motion field to sparse, 1-D data constraints. In our approach, the finite element model is used as a numerical method of solving dynamic system equations derived from continuum mechanics models and image-based constraints.

More recently, the UPenn group has been moving toward the use of locally deformable superquadrics models based on the work of Metaxas [31] as the parameterized model that can be used as the unifying approach to assemble the MR tag (SPAMM) data. This provides an interesting and possibly robust basis upon which to gather this information, and the investigators note that global motion parameters of interest can be extracted [31]. This work has typically proceeded using MR tag data in the mid-wall, although the authors imply that they are moving toward a 3D model using boundary constraints to try to create a fully transmural strain map. However, due to the x-y grid nature of the SPAMM tags, the only truly reliable, corresponded displacement information will tend to come from the mid-wall tag sites. This means that in any

one spatial slice, point- tracked LV function measures such as strain are quite accurate in the mid- LV wall region, but tend to be noisy and inaccurate near the endocardial and epicardial boundaries, as the grids cross over into the LV blood pool or the pericardial space.

At Johns Hopkins University, several efforts aimed at assembling 3D maps of myocardial deformation are ongoing, using the radial MR tagging scheme developed there. In [30], the authors utilize an MR acquisition sequence that obtains 3D tag information one component at a time, again generating a sparse set of corresponded tag points. They propose fitting a high-order polynomial to the displacement field in order to interpolate between the sparse data points. Alternatively, the authors in [8] propose an estimation theory- based idea that uses a stochastic vector field to assist in the interpolation. The authors argue that their approach uses fairly weak assumptions on the specifics of heart wall motion as compared to some of the other techniques mentioned above, and the Fisher estimate that is used in their approach can help them relate estimation accuracy to the number of tag lines needed. On the down side, their approach actually increases the errors at the boundaries of the myocardium, according to their phantom studies.

While some of the approaches described above are related to our continuum model–based approach described below, these ideas are geared toward dealing exclusively with MR tagging data, whereas our goals are to develop techniques useful with data from one of several different modalities. Also, while there is no doubt that MR tagging potentially provides unique and interesting data regarding LV myocardial movement, the user should be cautioned that there are quite a few processing steps required to assemble the data into meaningful measures of 3D deformation even *after* the acquisition. Just having the MR tag data available *does not* in itself mean that physiologically/clinically accurate analysis is forthcoming. The proper choice of image analysis and processing algorithms for assembling these data remains a significant open question.

Shape-Based Estimates of LV Endocardial/Epicardial Surface Displacements. The bounding sur-

faces of the LV can be isolated in the image data using automated 3D segmentation techniques [39]. Once these operations are completed, one can compute the principal curvatures of local patches on each surface and use these as feature–based tokens for tracking surface motion in 3D space [6, 22]. An earlier form of the work performed by our group was described in [10], but more current descriptions are documented in [25, 38].

In our efforts, natural neighbor relationships between surface points are used to allow a multi-scale local surface representation for curvature calculation, depending on the curvedness of LV features expected in that region. Under the assumption that the surface patch surrounding each sample point $\mathbf{x}$ deforms only slightly and locally within a small time interval, a physically-plausible search region W is defined on the second surface at time t_{i+1} for each sampled point on the first surface at time t_i. Bending energy measures between the surface patch surrounding point $\mathbf{x}$ and surface patches surrounding candidate points are computed, and the point $\bar{\mathbf{x}}$ that has the *minimum* corresponding bending energy is chosen as the point corresponding to point $\mathbf{x}$. By matching the curvatures of surface patches that surround each sample point at time t with similarly–sized patches surrounding candidate points at time $t + 1$, a shape–based initial match result and matching confidence measure (the latter related to strength and uniqueness of the match) are obtained.

These initially calculated 3D displacement vectors can be noisy due to inherent noises from image data, segmentation, and curvature estimation, an intelligent smoothing process based on solving confidence- weighted- regularization functional is utilized to help limit these problems. The regularization functional incorporates the shape match and confidence measure information just mentioned and is described in detail in [38]. Solving this functional for each pair of surfaces, complete trajectories are then formed by concatenating these vectors over many frames.

Phase Contrast MRI- Based Analysis of Cardiac Deformation. Several investigators have employed changes in MR phase due to motion of tissue within a fixed voxel or volume of interest to assist in estimating instantaneous, localized velocities, and ultimately cardiac motion and

deformation. While the basic ideas were first suggested by van Dijk [41] and Nayler[29], it was Pelc and his team [33, 34, 32] that first bridged the technique to conventional cine MR imaging and permitted the tracking of myocardial motion throughout the cardiac cycle. This technique basically relies on the fact that a uniform motion of tissue in the presence of a magnetic field gradient produces a change in the NMR signal phase that is proportional to velocity. These velocities can then be integrated to estimate the pointwise displacement of a region of the myocardium. In principle, these instantaneous Eulerian velocities can be derived from each pixel in an image acquisition. However, clusters of pixels within regions-of- interest (ROI's) are typically analyzed when predicting pointwise motion, primarily due to signal-to-noise issues. Several investigators have studied the resolution and accuracy of these techniques for tracking myocardial motion and strain including the Stanford team (see [17]), Wedeen [44], Constable [7], and Meyer[27]. It is worth noting that, as with MR tagging, accurately tracking myocardial motion in 3D requires additional image processing, and little has been reported in the literature about this problem. Assembling the dense field phase velocity information into a complete and accurate 3D myocardial deformation map is a limiting problem to date for this technology. Furthermore, currently phase contrast velocity estimates near the endocardial and epicardial boundaries are extremely noisy due to the fact that the required size of an ROI for signal-to-noise purposes is so big that it includes information from outside the myocardial wall. Thus, the most accurate LV function information is obtained from the middle of the myocardial wall, and is least accurate near the endocardial and epicardial wall boundaries. Also, because of the artifacts created by the high speed blood flow within LV, there exists a horizontal band of noise across of image which covers the ventricle. Velocity data with that band is usually noisy and unreliable. Often a perpendicular imaging sequence is performed to partially solve this problem.

Computer Vision- Based Ideas Related to Non-rigid Motion and Deformation Analysis. Image-based quantifying the deformation of the LV could be seen as a two step process: first establishing correspondence between certain points on the LV at time t and time $t+1$ and second, using

these correspondences as a guide, solve for a complete mapping of the LV between any two time frames. This problem could be posed for the entire myocardium or just portions of it, such as the endocardial surface alone. There has been considerable effort in general on these two topics, although rarely have they been addressed together. One form of establishing correspondence is using the MR tags or integrating MR phase velocities as described above. As noted above, tracking these usually visible MR tags still requires some effort (e.g. [15]), becomes increasingly difficult as the tags decay, and the approaches often rely on computer vision strategies such as deformable contours (e.g. [1]). The following of MR phase velocity data in a reliable manner has proved to be a most challenging task at noted in [27]. As described above, another approach to establishing correspondence is to track shape- related features on the LV over time [22, 6, 38]. The mapping or embedding between two 3D objects or surfaces is a problem that has received much attention in the medical image analysis and computer vision communities. Efforts aimed at solving for a nonlinear mapping between two objects are most related to the cardiac tracking problem and include the work of [35], [5] and [40]. In [35], as well as interesting complementary work in [31] and [28], physically-based finite element models were used to provide a framework for the mappings. In all of these approaches, estimates of correspondence between individual points on objects were either specifically assumed to be known to aid in solving the problem, relied on some global distance measure, or was not considered at all in the solution. We have aggressively pursued the notion of trying to solve both the correspondence problem and the mapping problem from 3D frame to 3D frame as will be described below. We also note the efforts of Ayache, et al. [6] who discuss integrating shape matching and surface mapping. We point out that no work has been reported to date that has merged the computer vision- like notions of shape- matching and nonlinear registration with the more image acquisition- physics-based concepts such as MR phase- velocity within a unified framework as will now be described.

Another fundamental issue in the analysis of clinical images of ventricular wall motion is the principle of frame indifference. In other words, it is often preferred in regional function analysis to measure object-centered deformation parameters such as strains, as opposed to

frame-centered parameters such as displacements or velocities. One main advantage is that whereas strain is independent of translation and rotation, velocity and displacement are not. Hence, our main goal in our model-based, integrated framework is to derived local deformation from image sequences.

A Unified Framework for Estimating LV Motion and Deformation Based on Continuum Mechanics

We now form a framework from which we can compute myocardial deformation by integrating image-derived displacement and velocity data considered separately by others and described above. While we choose to explain our approach using shape-based boundary displacement data and mid-wall velocity data, it is of interest to note that any of the image-derived data described in the previous section can be employed here. Also note that in each modality the images from which we derive the two sources of data are perfectly registered with each other. For instance in the main dataset we work with, they are components of the same complex MR signals. The LV model represents an imaged myocardial 3D section as a homogeneous elastic solid continuum bounded by the endocardial and epicardial surfaces found using the above-mentioned segmentation strategies. Figure 1 illustrates the myocardial volume we are using, as well as the regions where shape displacement and mid-wall velocity data will be incorporated.

The heart has some rather complex biomechanical properties in general and others have developed sophisticated models to capture this. In our work aimed at beginning to bridge these models into the image analysis problem, we set out to use simple, but plausible, model forms that will be computationally feasible. Thus for our initial 3D efforts here, we assume that the myocardium is a linear material, with its stress-strain relationship (the constitutive equation of the material) obeying *Hooke's law*: $[\sigma] = [D][\varepsilon]$, where $[D]$ is a 6x6 matrix that is a function of the *Young's modulus*, a material specific constant which has been established experimentally for the canine myocardium in the biomechanics literature[45] to be around 75,000 Pascal, and *Poisson's ratio*, another material related constant set to approximately 0.5 for incompressible

material. We do want to point out that we are currently investigating in detail the incorporation of more sophisticated constitutive models that have already been explored by the biomechanics community for non-image analysis- based work, such as those of Humphrey [19] and Guccione [14], any of which can be inserted into this framework. After we establish the strain–stress relationship, we incorporate it into the numerical solution of the integrated motion recovery using a finite element framework.

The finite element method is a numerical technique for analyzing the dynamic behavior of an object. The first step in this method is to divide the continuous structure of the object into finite pieces, or *elements*, and to construct a finite element mesh to represent the continuous object. We create a fully three- dimensional finite element mesh that tessellates the complete thickness of the left ventricular myocardium at any one 3D image frame. It has nodes in the mid-wall region, as well as nodes on the endocardial and epicardial surfaces. The 3D grid that will constitute the LV model is formed as follows: first the epicardial and endocardial surfaces are found by segmentation technique [39]. Next, a bounded and constrained Delaunay triangulation technique is used to form a fairly dense tessellation. A solid finite element LV model which consists of many tetrahedra is thus generated for any one time frame, with linear basis functions [4] constructed for each element. An isoparametric formulation is used, so that the interpolation of the element coordinates and element displacements use the same basis functions, and it is all defined in a natural coordinate system. Finally, regarding the formulation of this initial grid, we note that to reduce the spatial extent of the acquisition as well as both acquisition and computation time, we have limited the construction of the 3D FEM mesh to a section of the myocardium defined along the LV long axis that contains image slices from the middle of the LV down to just above the apex.

We derive the governing equations of the dynamics of the three-dimensional myocardium using the minimum potential energy principle, based on the isotropic linear elastic model. We

assemble the equations together, and write them in matrix form as:

$$\mathbf{M}\ddot{\mathbf{U}} + \mathbf{C}\dot{\mathbf{U}} + \mathbf{K}\mathbf{U} = \mathbf{R} \tag{1}$$

where $\mathbf{M}$ is the mass matrix, $\mathbf{C}$ is the damping matrix, $\mathbf{K}$ is the stiffness matrix, $\mathbf{R}$ is force load, and $\mathbf{U}$ is the nodal displacement vector field. The mass matrix $\mathbf{M}$ is a function of the element basis function and the assumed material density (see [45]), which are both known. The stiffness matrix $\mathbf{K}$ is a function of element basis function and material strain-stress relationship matrix defined above, so it is also known. Meanwhile, the damping matrix $\mathbf{C}$ represents viscous damping, and we use a common spectral damping scheme, the Rayleigh damping, to approximate $\mathbf{C}$ as a linear combination of the mass and stiffness matrices. Currently, we assume the system to be a low damping system with a low frequency content, and as a result approximate $\mathbf{C}$ to be proportional only to the mass and to be about one percent of the value of the corresponding element of $\mathbf{M}$. Further, we want to point out that we intend to use this model to enforce certain real physical constraints that we obtain through measurements of cardiac volumes and pressures.

To this point we have constructed a transmural 3D finite element representation of the LV which has nodes in the mid-wall regions and on the bounding endocardial and epicardial surfaces, and in addition have also established the general governing equations of the entire biomechanical system model. The framework is formulated such that the mid-wall velocity and the boundary displacements are used as data-based constraints. The unknown field variables are the displacement vectors at the nodal points, although the derivatives of the displacements (velocity and acceleration vectors at the nodal points) can also be derived from the system equations.

We first set up the initial conditions for the complete system of differential equations for any starting time instant (say t). We assume that the initial displacement of all the points $\mathbf{U}(\mathbf{t})$ would always be zero as the object has not moved yet. Since we have been encouraged that the incorporation of a model of the generally cyclical motion of the LV into our shape-

based tracking procedure has improved our (2D) algorithm's estimates of point-wise motion[25], we intend to constrain the motion of each and every point in the final 3D FEM grid to being cyclical in nature., which is often neglected by other approaches. Next, the MR phase contrast data at this starting instant provides the initial velocity information $\dot{\mathbf{U}}_{mid-wall}(t)$ of the mid–wall region (the mid–wall region is defined as consisting of points that are at least one pixel away from the segmented endocardial and epicardial surfaces). For the remaining points, we assume $\dot{\mathbf{U}}_{other}(t)$ is zero. However, if we take into account the periodic nature of the heart motion, we may use the estimated velocity at these points from the solution of equations at the previous time instant as the initial velocity at this time. The initial acceleration of all the points $\ddot{\mathbf{U}}_{all}(t)$ is set to zero. The initial equivalent total load $\dot{\mathbf{R}}(t)$ can thus be computed from the governing equations: $\mathbf{R(t)} = \mathbf{M\ddot{U}(t)} + \mathbf{C\dot{U}(t)}$ where $\dot{\mathbf{U}}(t)$ and $\ddot{\mathbf{U}}(t)$ are already known. We also want enforce the displacements of the sampled boundary points $\mathbf{U}_{boundary}(t+dt)$ when the myocardium deforms into the next time instant $t+dt$. One way to include these prescribed nodal displacements while retaining the original structure of system equations is to modify certain diagonal terms of the stiffness matrix $[K]$ and the corresponding terms of the load vector $[F]$. The approach we take to incorporate this constraint is as follows: assume that the ith node has enforced displacement b, then we multiply the ii^{th} element of the stiffness matrix $\mathbf{K}$ by N , and the ith element of the load vector $\mathbf{R}$ is replaced by $N*b$ where N is very large. Following this manipulation, the modified governing equations must now yield $\mathbf{U}_i(t+dt) = b$. Physically, this procedure can be interpreted as adding a spring of vary large stiffness, and specifying a load which produces the required displacement b for variable U_i. This procedure is repeated until all prescribed displacement variables have been treated. After these modifications have been made, we proceed with the simultaneous solution to the complete set of differential equations. In very strict terms, this modifying procedure will not give the exact values for the prescribed displacements at the corresponding nodal points because we have only modified the $[K]$ and $[F]$ matrices but not the $[M]$ and $[C]$ matrices. However, if the chosen large multiplying factors are indeed very large compared to the values of the matrix terms, the errors

will be negligible. In addition, this inexactness provides a way of incorporation of confidence measures into the displacement boundary conditions. Since we are using the displacement between shape- matched points as the prescribed displacements in the unified framework, we treat these displacements differently based on their confidence measures. From this point of view, the large multiplying factor is weighted by the confidence measure for each prescribed displacement. The displacements with high confidence measures have *really large* multiplying factors to enforce the system solution to give the exact prescribed values at these nodal points. The displacements with low confidence measures often have relatively small multiplying factors to have inexact solution values, which are the compromise of the prescribed conditions and the smoothness constraint which is implicitly enforced by the constitutive laws of the materials.

Through the construction of the initial conditions, and the enforcement of the shape- based boundary landmark displacements, the solution to the governing equations yields a predicted set of displacements, velocities and accelerations at time $t + dt$ that are the results of the integration of two sources of image–derived information under the guidance of the physical model. The step–by–step solution of the system is performed using the Newmark integration method, which is unconditionally stable [4] (the time step dt is governed only by considerations of accuracy which for low frequency systems can be fairly large to obtain accurate results). This model thus represents a continuous description of the entire left ventricle at any one time frame and it's predicted deformation to a second time frame given a set of image-data- based displacements and velocities.

We note that the finite element framework acts as a predictor for our system. Since we already have geometrical information at $t + dt$ in terms of the segmented endocardial and epicardial surfaces, as well as the velocity information of mid-wall points at $t + dt$ from phase contrast images, we can refine the mapping estimate between frames t and $t + dt$ by seeing how close the displacement/velocity driven, model–based prediction comes to the actual segmented surfaces and actual instantaneous velocities. The differences between the actual data and the

prediction are then used as a recursive feedback term to improve the estimate of the deformation mapping between frames. In [37], we reported our progress in using differences in coarse scale 2D boundary difference as the feedback force. Currently, we are work on utilizing both 3D surface shape differences and velocity differences between the actual data at frame $t + dt$ and the prediction for that frame in the correction scheme. Initially, we create two metrics that minimize these differences by adjusting the displacements (thus, the velocities will first be integrated) of the nodes in the predicted mesh, each within a spatially limited search region. Surface shape is compared at a coarse scale, and performed where there are key features for tracking occur. Integrated mid-wall phase contrast velocities are compared at regularly sampled intervals and broader regions than in the prediction computation. The intent is that in the end a fairly sparse set of mesh nodes will be adjusted, with the idea that this will be sufficient to provide some error correction without a great computational burden. Furthermore, we are moving towards using Kalman statistical filtering framework that we used successfully in [27] into the 3D prediction models.

Deriving Quantitative Measurements. Previously, we have looked at endocardial motion and endocardial- epicardial thickening as quantitative measures of LV function. It is now our sense that all of these measures are simply portions of a more complete description of the mechanical deformation of the LV, namely point–tracked, myocardium–referenced measures of LV strain, known as the Lagrangian strain. A complete 3D characterization of strain better answers the basic question of how the mechanical function of the LV varies regionally, and how it's altered under a variety of normal and abnormal (especially acute infarct) conditions. Assuming the Hookean model described above that we use in our effort, the Lagrangian strain tensor that can be derived for each and every portion of the FE mesh contains 6 components [12]. More cardiac specific strains, i.e. longitudinal, circumferential, and radial, as well as strains along fiber directions can also be derived.

Experimental Results. The integrated motion and deformation analysis framework proposed

has been implemented. Experiments have been conducted with cardiac MR phase contrast images acquired from fasting anesthetized, open chest, adult mongrel dogs. The canine heart was exposed through a thoracotomy. The proximal portion of the left anterior descending (LAD) coronary artery was isolated for placement of a snare occluder.

The results of the shape-based surface motion tracking have been shown in figure 2(a-g) on a MRI dataset of canine study. Each of the sixteen image volumes has an in-plane resolution of $1.64mm/pixel$ and inter-plane resolution of $5mm/pixel$. Figure 2(a-d) illustrates the bending energies (shape features) that were computed at the end- diastolic (ED) endocardial surfaces and three successive time frames after ED for typical MRI baseline studies. A few of the trajectories that were computed for these surfaces are noted in figure 2(e-f). Trajectories of isolated surface points are compared to the trajectories of implanted imaging opaque makers (four endocardial, four epicardial), and the average positional errors are within image resolution for sixteen datasets [38]. We also note that we were able to track related sets of endocardial/ epicardial points (useful for strain computation), as shown in figure 2g.

Figure 3 shows an example of phase contrast images of a canine study. In this dataset, three contiguous short axis slices were collected using the cine phase contrast gradient echo sequence for sixteen time frames. The imaging parameters were: flip angle = $30°$, $TE = 34msec$, $TR = 34msec$, $FOV = 28cm$, $5mm$ skip 0, matrix 256x128, 4 nex, venc = $15cm/sec$. The in-plane resolution of the dataset is $1.09mm/pixel$, and the inter-plane resolution is $5mm$. The intensity values of the velocity images range from $-150mm/sec$ to $150mm/sec$, with the signs of the values indicating the directions of the velocities. The dog's LAD coronary artery was occluded to cause dyskinetic motion at the inter-ventricular septum (the lower left part of the LV). It should also be noted that because of the time (ten to fifteen minutes) to acquire each set of directional phase velocity images (three slices are acquired at each time), the image dataset only covers a small part of the left ventricle. However, this does not alter the validity of using this dataset to test the capability of the integrated framework except that there is 3D motion

out of the field of view vertically.

Since it is more desirable to have roughly equal resolutions in all three dimensions to track surface motion, interpolation is needed between the data contour slices. A chamfer distance based contour interpolation is used to insert three interpolated contours to every two consecutive data contours [18]. The shape-based surface motion tracking process is then applied to the sixteen interpolated surface sequences, once for the endocardium and once for the epicardium. This way, the surface displacements have $1.09mm$ in-plane resolution and $1.25mm$ inter-plane resolution. A subset of the surface point displacements (10 %) are used as the boundary displacement constraints in the integrated volumetric framework.

The mid-wall velocities of the phase contrast images are used as the initial velocity constraints in the integrated volumetric framework. For computational reasons, the myocardial surfaces are re-sampled to the lower resolutions of $4.36mm/pixel$ in-plane and $5mm/pixel$ inter-plane after the surface motion tracking has been performed. This way, even though the final re-sampled dataset has only $4.36mm$ in-plane and $5mm$ inter-plane resolutions to form larger tetrahedral elements to save computational expense, the boundary displacements still have $1.09mm$ in-plane and $1.25mm$ inter-plane resolutions. It should be noted that higher resolution gives smoother and more accurate geometrical representation of the LV, although it will require much more computer power. The myocardial sample points which are bounded by the endocardial and epicardial boundaries are Delaunay tessellated to form the finite element mesh of the myocardium. Figure 4 shows the low resolution tetrahedral finite element mesh of the mid-ventricle covered by the three-slice image set. In this case, there are 2147 tetrahedra in the mesh.

Following the procedures established in the previous sections, the governing equations of the myocardium are derived from the minimum potential energy principle. A linear isotropic elastic myocardial model is used, and the material-related constants that have been established experimentally for the myocardium in the biomechanics literature [45] are used. The velocity

values at the mid-wall points are used as the initial velocity conditions, and the surface displacements are used as the displacement boundary conditions. Since the temporal resolution of the dataset is $0.03125sec/frame$, we choose the integration time step $\Delta t = 0.003125sec$ to have 10 integrated steps. Using these constraints and parameters, the motion and deformation parameters of the myocardium at all sixteen time frames are calculated using the Newmark integration process. The required computer memory for the system to handle this data set is around 60MB. The computation time for each pair of images is about half an hour on a Silicon Graphics HighImpact workstation with 195 MHZ R10000 processor and 128MB memory.

Figure 5 presents the two-dimensional projection of the three-dimensional dense field displacement vector map of the middle slice from ED to the next time frame, found from the integrated framework. The use of 2D projections instead of a true 3D vector map is only because of the ease of visualization. Here, a vector arrow begins from its position at present time (ED), and ends at its position in the next time frame. The non-homogeneous nature of the myocardial motion is very evident from this displacement map: different regions of the myocardium display very different motion characteristics in direction and magnitude.

We have also calculated the strain tensors for each tetrahedral element of the finite element grid to depict the non-rigid deformation. Figure 6 shows the maximum principal strain map of the myocardium, as well as the two-dimensional projections of the associated three-dimensional directions at the middle slice. The strains shown are mapped back to the myocardial grid at its original state (ED). In the figure, the strain values are represented by different shades of red, where darker red represents higher strain. Also, we want to point out the apparent non-uniform strains transmurally across the heart wall, which could be extremely important in validating the clinical observations that the ischemic disease progresses transmurally overtime. Of course, any significant claim can only be made after more carefully designed validation on a range of image datasets. Figure 6d shows a cutaway view of the maximal principal strain map at ES with respect to ED. Figure 7 shows the temporal sequence of the first principal strain maps

from ED to ES. Note the different strain values between different regions. We find that the anterior septal region has the highest average maximum principal strain, which coincides with the injury region observed from post mortem TTC staining. Also, we observe that the average value of the first principal strain reaches a maximum strain of 32% at ES, the average second strain is very small and stable, and the third principal strain reaches -18% at ES, all values are in rough agreement with the strain ranges estimated from MR tagging based approaches as well as those from biomechanics literature.

In addition, we are currently looking into the possibility of calculating strains in the myofiber directions which have been documented [20]. This way, it can not only more accurately and meaningfully compute and interpret the strain information, it can also facilitate the plan of measuring active myocardial tension development.

Conclusions

Recovering a dense field of LV strain values from image data remains a challenging but important problem. A variety of work is going on in the medical imaging/image analysis community as was discussed in the Overview section. We have discussed in detail in this paper one approach that uses integrated framework for the analysis of left ventricular motion and deformation. This unified approach is based upon the use of image analysis strategies and mechanical modeling of the myocardium, and is embedded in a finite element framework for the integration of complementary image sources. Experiments have been performed on canine MR phase contrast images. Motion and deformation parameters are estimated from the integration of boundary displacement information and mid-wall phase velocity information.

Ongoing and future work includes adopting more sophisticated continuum biomechanical models of the myocardium based on the theory of finite deformation. Temporal periodic characteristics of the heart motion as well as 3D feedback mechanism will also be incorporated into the current framework. In addition, while we have been focusing on the use of biomechani-

cal models to aid heart motion and deformation recovery from images, we also begin to look into the potential of deriving fundamental properties of the myocardium, such as strain energy and material characteristics, from image- based framework. While our current approach may provide useful clinical or diagnostic tools, image- derived material properties will contribute to a more basic understanding of the myocardial biophysics and physiology. Towards this goal, we believe that frameworks with stochastic dynamic characteristics, for both image data and the myocardial models, are needed in order to achieve optimal estimate of state for particular *a priori* physical models and *a posteriori* image data. For problems involved time-dependent information such as motion, stochastic dynamics also provides ways of incorporate temporal constraints into the framework.

References

[1] A. Amini, P. Shi, T. Constable, K. Johnson, J. Duncan, and J. Gore. Energy- minimizing deformable grids for tracking tagged MR cardiac images. In *Computers in Cardiology*, Durham, N.C., Oct 1992.

[2] L. Axel and L. Dougherty. MR imaging of motion with spatial modulation of magnetization. *Radiology*, 171:841–845, 1989.

[3] H. Azhari and et. al. Noninvasive quantification of principal strains in normal canine hearts using tagged MRI images in 3d. *Am. J. Physiol.*, 264:H205–H216, 1993.

[4] K. Bathe and E. Wilson. *Numerical Methods in Finite Element Analysis*. Prentice Hall, 1976.

[5] F. Bookstein. A geometric foundation for the study of left ventricular motion: Some tensor considerations. In A. Buda and E. Delp, editors, *Digital Cardiac Imaging*, pages 65–83, 1985.

[6] I. Cohen, N. Ayache, and P. Sulger. Tracking points on deformable objects using curvature information. In *Lecture Notes in Computer Science- ECCV92*, pages 458–466. Springer Verlag, 1992.

[7] T. Constable, K. Rath, A. Sinusas, and J. Gore. Development and evaluation of tracking algorithms for cardiac wall motion analysis using phase velocity MR imaging. *Magn. Reson. Med.*, 32:33–42, 1994.

[8] T. Denney and J. L. Prince. 3d displacement field reconstruction from planar tagged cardiac MR images. In *Workshop on Biomedical Image Analysis*, pages 51–60, Seattle, Washington, 1994.

[9] J. M. Dieudonne. Gradients de directions et la deformations principales dans la paroi ventriculaire gauch normale. *J. Physiol. Paris*, 61:305–330, 1969.

[10] J. S. Duncan, P. Shi, and et al. Towards reliable, noninvasive measurement of myocardial function from 4d images. In E. Hoffman and R. Acharya, editors, *Medical Imaging 1994: Physiology and Function form Multidimensional Images*, pages 149–161, Newport Beach, Feb 1994. SPIE.

[11] T. Freeman, J. Cherry, and G. Klassen. Transmural myocardial deformation in the canine left ventricular wall. *Am J. Physiology*, 235:H5230–H530, 1978.

[12] Y.C. Fung. *A First Course in Continuum Mechanics*. Prentice- Hall, Inc., Englewood Cliffs, N.J., 1969.

[13] K. Gallagher, G. Oksada, M. Miller, W. Kemper, and J. Ross. Nonuniformity of inner and outer systolic wall thickening in conscious dogs. *Am J. Physiology*, 249:H241–H248, 1985.

[14] J. M. Guccione, A. D. McCulloch, and L. K. Waldman. Passive material properties of intact ventricular myocardium determined from a cylindrical model. *Journal of Biomechanical Engineering*, 113:42–55, 1991.

[15] M. Guttman, J. Prince, and E. McVeigh. Tag and contour detection in tagged MR images of the left ventricle. *IEEE Trans Med Imaging*, 13(1):74–88, 1994.

[16] A. R. Hashima, A. A. Young, A. D. McCulloch, and L. K. Waldman. Non-homogeneous analysis of epicardial strain distributions during acute myocardial ischemia in the dog. *Journal of Biomechanics*, 26(1):19–35, 1993.

[17] R. Herfkens, N. Pelc, L. Pelc, and J. Sayre. Right ventricular strain measured by phase contrast MRI. In *Proceedings of the 10th Annual SMRM*, page 163, San Francisco, 1991.

[18] G. T. Herman, J. Zheng, and C. A. Bucholtz. Shape-based interpolation. *IEEE Computer Graphics and Applications*, pages 69–79, 1992.

[19] J. D. Humphrey and F. C. P. Yin. Biomechanical experiments on excised myocardium: theoretical considerations. *Journal of Biomechanics*, 22:377–383, 1990.

[20] P. Hunter, A. McCulloch, P. Nielsen, and B. Smaill. A finite element model of passive ventricular mechanics. In R. Spilker and B. Simon, editors, *Computational Methods in Bioengineering*, pages 387–397. ASME, 1988.

[21] N. Ingels, G. Daughters, E. Stinson, and E. Alderman. Measurement of midwall myocardial dynamics in intact man by radiography of surgically implanted markers. *Circulation*, 52:859–867, November 1975.

[22] C. Kambhamettu and D. Goldgof. Curvature- based approach to point correspondence recovery in conformal nonrigid motion. *CVGIP: Image Understanding*, 60(1):26–43, July 1994.

[23] D. King, A. Gopal, A. Keller, and et al. Three- dimensional echocardiography: Advances for measurement of volume and mass. *Hypertension*, 23(suppl. I):I172–I179, 1994.

[24] A. McCulloch and J. Omens. Non-homogeneous analysis of three- dimensional transmural finite deformation in canine ventricular myocardium. *Journal of Biomechanics*, 24(7):539–548, 1991.

[25] J. C. McEachen and J. S. Duncan. Shape-based tracking of left ventricular wall motion. *IEEE Trans. on Med. Imag.*, 16:270–283, 1997.

[26] G. D. Meier, M. Ziskin, W. P. Santamore, and A. Bove. Kinematics of the beating heart. *IEEE Trans Biomed Eng*, 27:319–329, 1980.

[27] F. Meyer, T. Constable, A. Sinusas, and J. Duncan. Tracking myocardial deformation using spatially- constrained velocities. *IEEE Trans. on Med. Imag.*, 15:453–465, 1996.

[28] C. Nastar and N. Ayache. Classification of nonrigid motion in 3d images using physics-based vibration analysis. In *Workshop on Biomedical Image Analysis*, pages 61–69, Seattle, Washington, 1994.

[29] G. Nayler, N.Firmin, and D. Longmore. Blood flow imaging by cine magnetic resonance. *J. Comp. Assist. Tomog.*, 10:715–722, 1986.

[30] W. Odell, C. Moore, and E. McVeigh. Displacement field fitting approach to calculate 3d deformations from parallel tagged grids. *J. Mag. Res. Imag.*, 3:P208, 1993.

[31] J. Park, D. Metaxas, and A. Young. Deformable models with parameter functions: Application to heart wall modeling. In *Computer Vision and Pattern Recognition (CVPR94)*, pages 437–442, Seattle, Washington, 1994.

[32] N. Pelc, R. Herfkens, A. Shimakawa, and D. Enzmann. Phase contrast cine magnetic resonance imaging. *Magn. Res. Quart.*, 7(4):229–254, 1991.

[33] N. J. Pelc. Myocardial motion analysis with phase contrast cine MRI. In *Proceedings of the 10th Annual SMRM*, page 17, San Francisco, 1991.

[34] N. J. Pelc, R. Herfkens, and L. Pelc. 3d analysis of myocardial motion and deformation with phase contrast cine MRI. In *Proceedings of the 11th Annual SMRM*, page 18, Berlin, 1992.

[35] S. Pentland and B. Horowitz. Recovery of nonrigid motion and structure. *IEEE Transactions on Pattern Analysis and Machine Intelligence*, 13(7):730–742, July 1991.

[36] F. Sheehan, D. Stewart, H. Dodge, S. Mitten, E. Bolson, and G. Brown. Variability in the measurement of regional left ventricular wall motion. *Circulation*, 68(3):550–559, 1983.

[37] P. Shi, G. Robinson, R. T. Constable, A. Sinusas, and J. Duncan. A model-based integrated approach to track myocardial deformation using displacement and velocity constraints. In *Fifth International Conference on Computer Vision*, pages 687–692, 1995.

[38] P. Shi, A. J. Sinusas, R. T. Constable, E. Ritman, and J. S. Duncan. Point-tracked quantitative analysis of left ventricular motion from 3d image sequences. *IEEE Transactions on Medical Imaging*, accepted.

[39] L. H. Staib and J. S. Duncan. Model-based deformable surface finding for medical images. *IEEE Transactions on Medical Imaging*, 15(5):720–731, 1996.

[40] R. Szeliski and S. Lavallee. Matching 3d anatomical surfaces with non- rigid deformations using octree splines. In *Workshop on Biomedical Image Analysis*, pages 144–153, Seattle, Washington, 1994.

[41] P. van Dijk. Direct cardiac NMR imaging of heart wall and blood flow velocity. *J. Comp. Assist. Tomog.*, 8:429–436, 1984.

[42] L. Waldman, Y. Fung, and J. Covell. Transmural myocardial deformation in the canine left ventricle. *Circ Res*, 57:152–163, 1985.

[43] L. K. Waldman. Multidimensional measurement of regional strains in the intact heart. In L. Glass, P. Hunter, and A. McCulloch, editors, *Theory of Heart*. Springer-Verlag, 1991.

[44] V. Wedeen. Magnetic resonance imaging of myocardial kinematics: Technique to detect, localize and quantify the strain rates of active human myocardium. *Magn. Reson. Med.*, 27:52–67, 1992.

[45] H. Yamada. *Strength of Biological Material*. Williams and Wilkins Co., 1970.

[46] A. A. Young and L. Axel. Three- dimensional motion and deformation of the heart wall: Estimation with spatial modulation of magnetization- a model- based approach. *Radiology*, 185:241–247, 1992.

[47] A. A. Young, P. J. Hunter, and B. H. Smaill. Epicardial surface estimation from coronary cineangiograms. *Computer Vision, Grpahics, and Image Processing*, 47:111–127, 1989.

[48] A. A. Young, D. Kraitchman, and L. Axel. Deformable models for tagged MR images: Reconstruction of two- and three- dimensional heart wall motion. In *Workshop on Biomedical Image Analysis*, pages 317–323, Seattle, Washington, 1994.

[49] E. Zerhouni and et. al. Tagging of the human heart by multiplanar selective RF saturation for the analysis of myocardial contraction. In *Abstracts of the Ann. Meeting of the Soc. of MR in Imaging*, page 10, San Francisco, 1988.
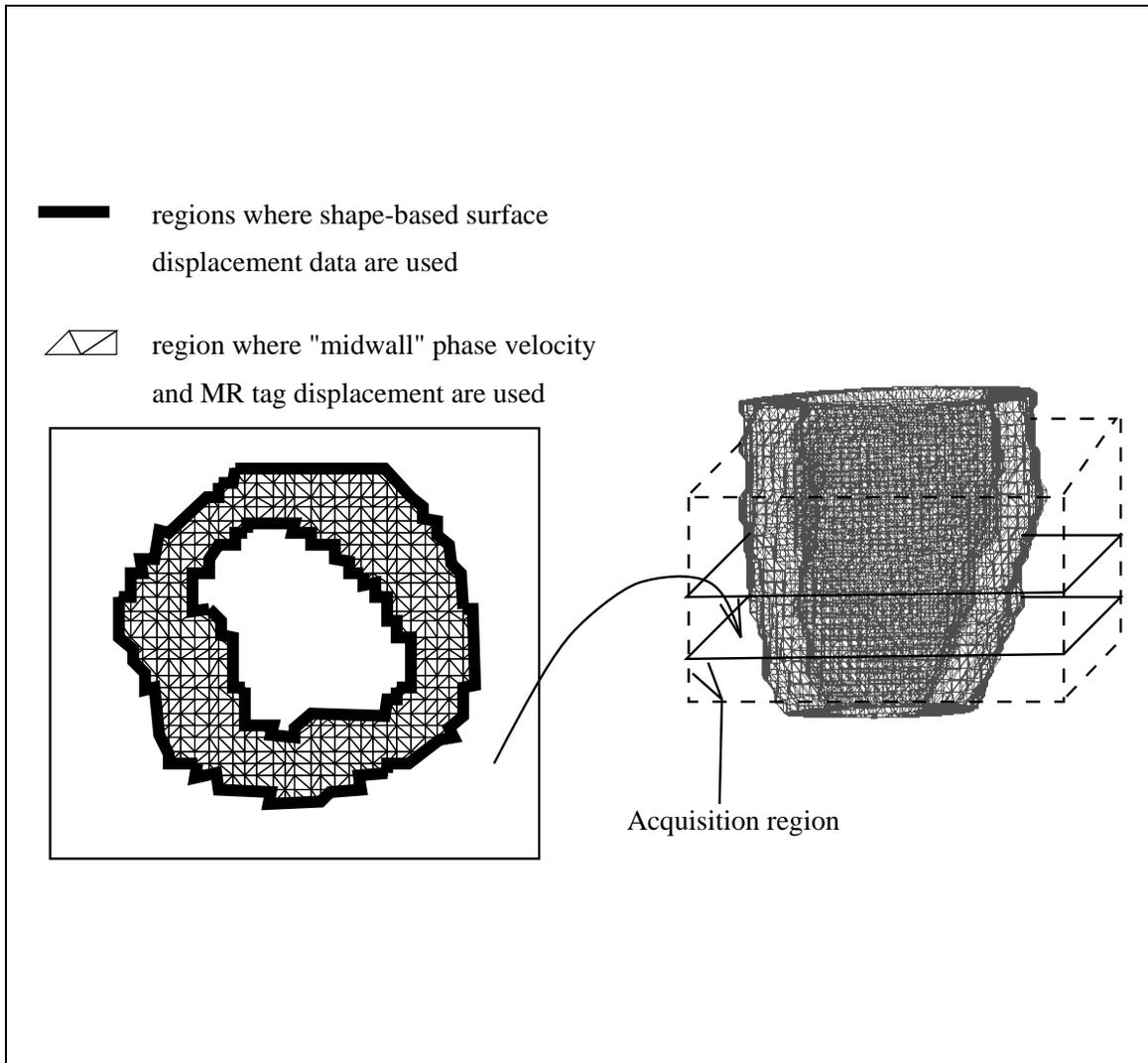
Figure 1: Right: Tessellated 3D myocardial section to be used in unified algorithm. Left: Cross section of finite element mesh showing regions where shape displacement and mid-wall velocity data will be incorporated.
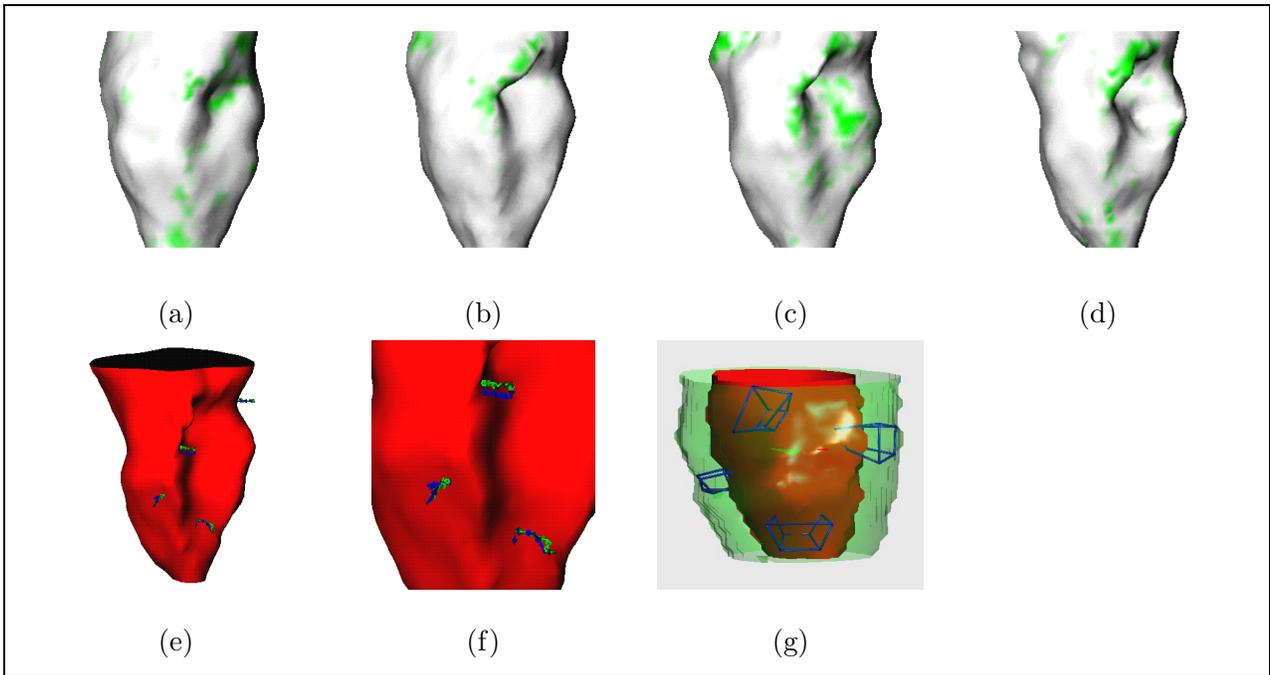
Figure 2: (a)–(d): Endocardial bending energies for the end-diastolic (ED) to ED+3 temporal frames for a MRI dataset. The color white represents flat region, and different shades of green represent degrees of bending energy, where darker green represents higher bending energy. (e): Algorithm-computed (blue) and implanted marker (green) trajectories starting at ED and moving to ES; (f): A blowup view of the trajectories shown in (e); (g): Related endocardial–epicardial point sets (transmural cubes).

(a)   (b)   (c)   (d)
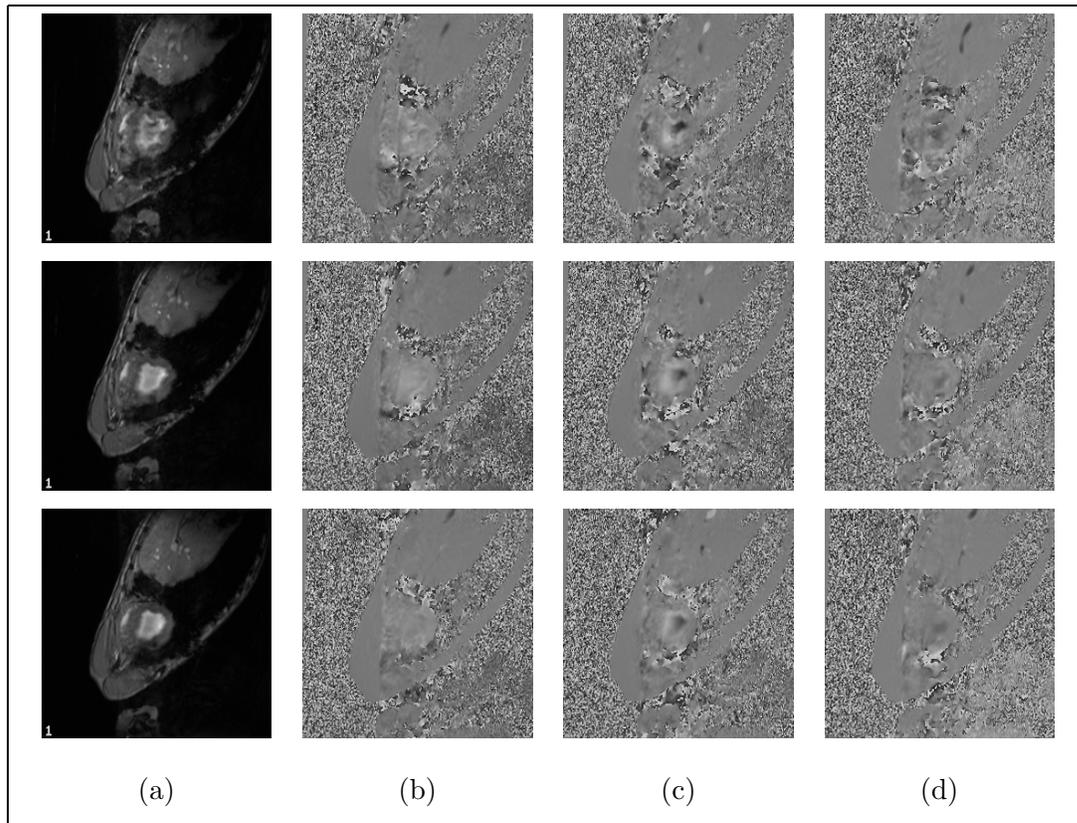
Figure 3: 3D MR phase contrast images at ED. Three mid–ventricle slices are acquired for sixteen time frames through the cardiac cycle. The top row shows the images of the slice which is closest to base, and the bottom row shows the images of the slice which is closest to apex. (a): the magnitude images which encode the anatomical structures; (b): images which encode x-direction velocities; (c): images which encode y-direction velocities; (d): images which encode z-direction velocities.
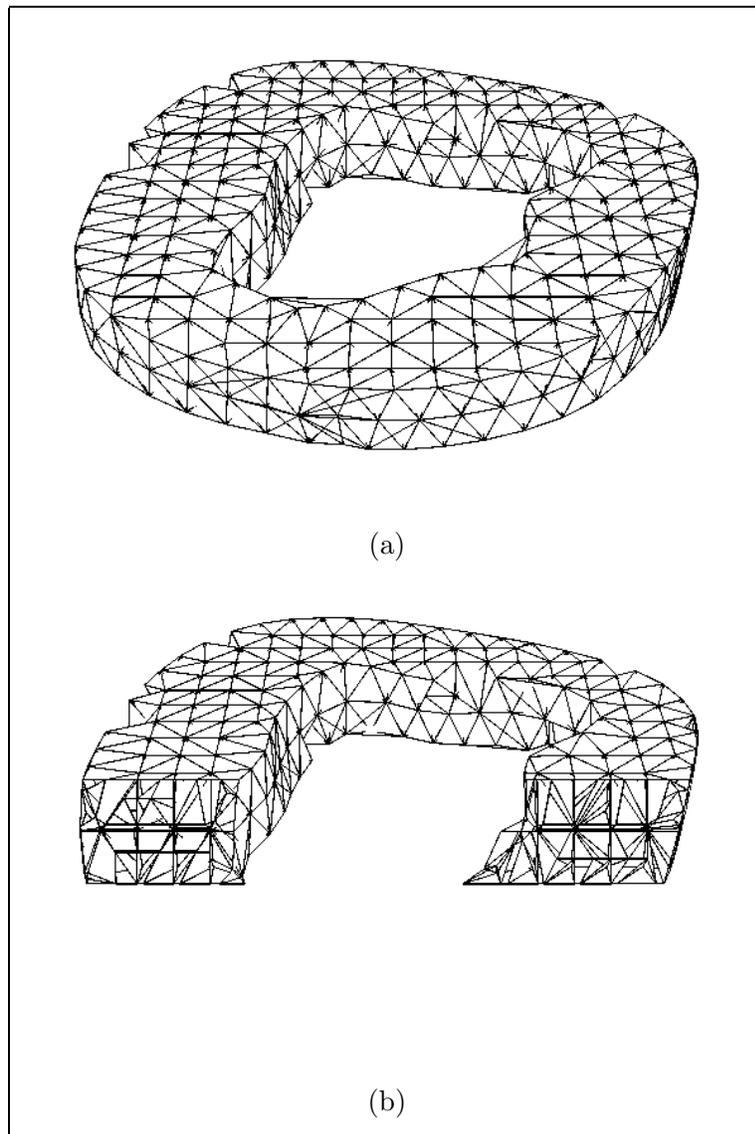
Figure 4: Volumetric finite element mesh of the mid-ventricle from phase contrast MR images. (a): overall view; (b): cutaway view.
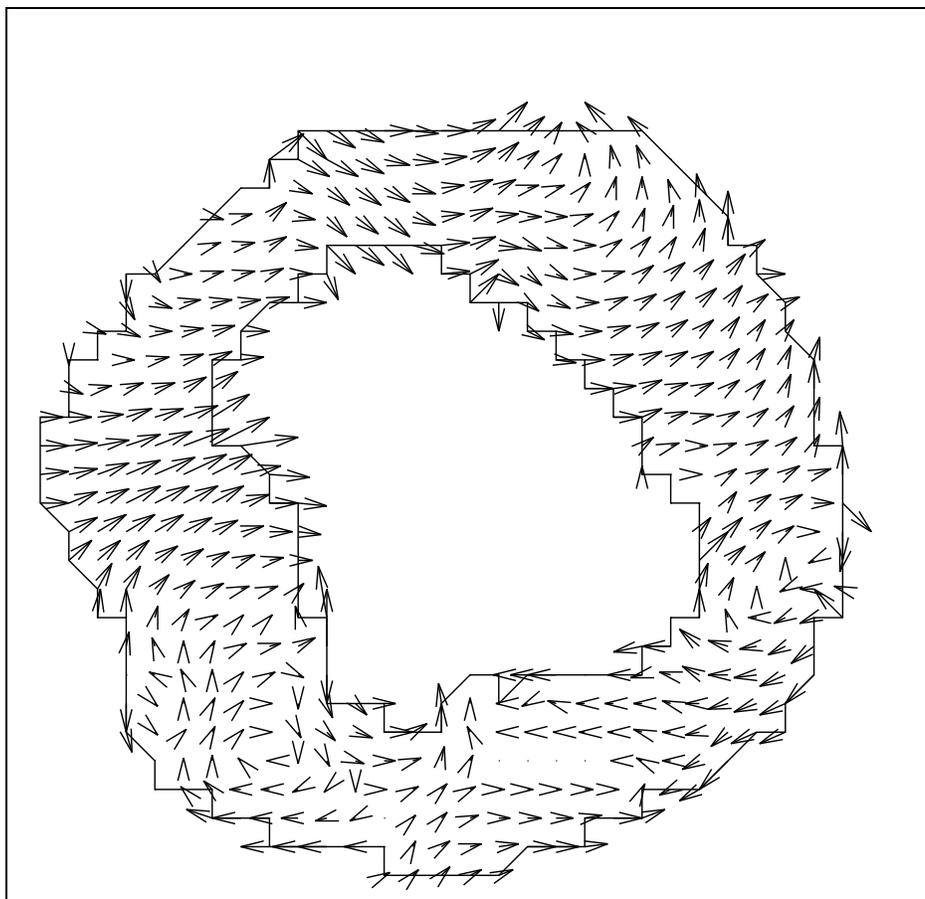
Figure 5: Dense field displacement vector map (2D projection) from the integrated framework.

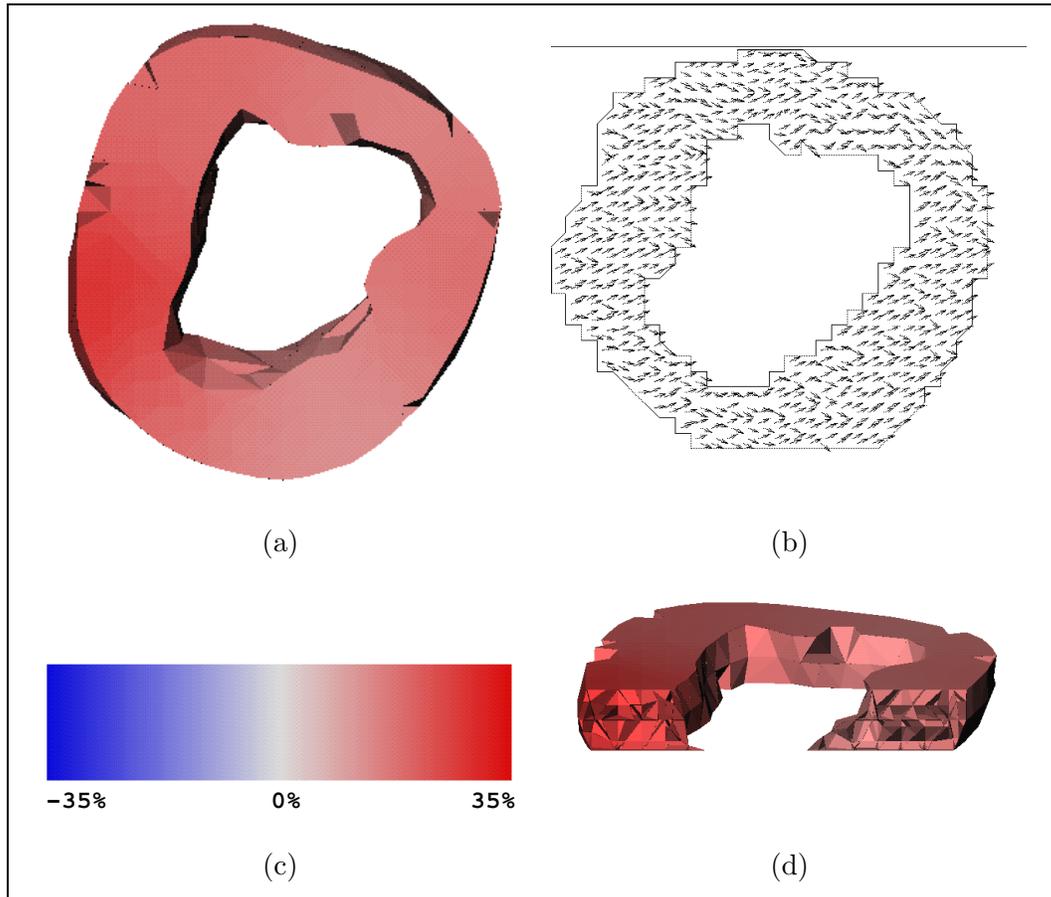Note the non-homogeneous nature of the myocardial motion.

Figure 6: 3D principal strain map of mid-ventricle (ED-ES). (a): the first (maximum) principal strain; (b): two-dimensional projections of the three-dimensional directions of the maximum principal strain (middle slice). (c): color scale for the first principal strain; (d): cutaway view of the maximal principal strain map.
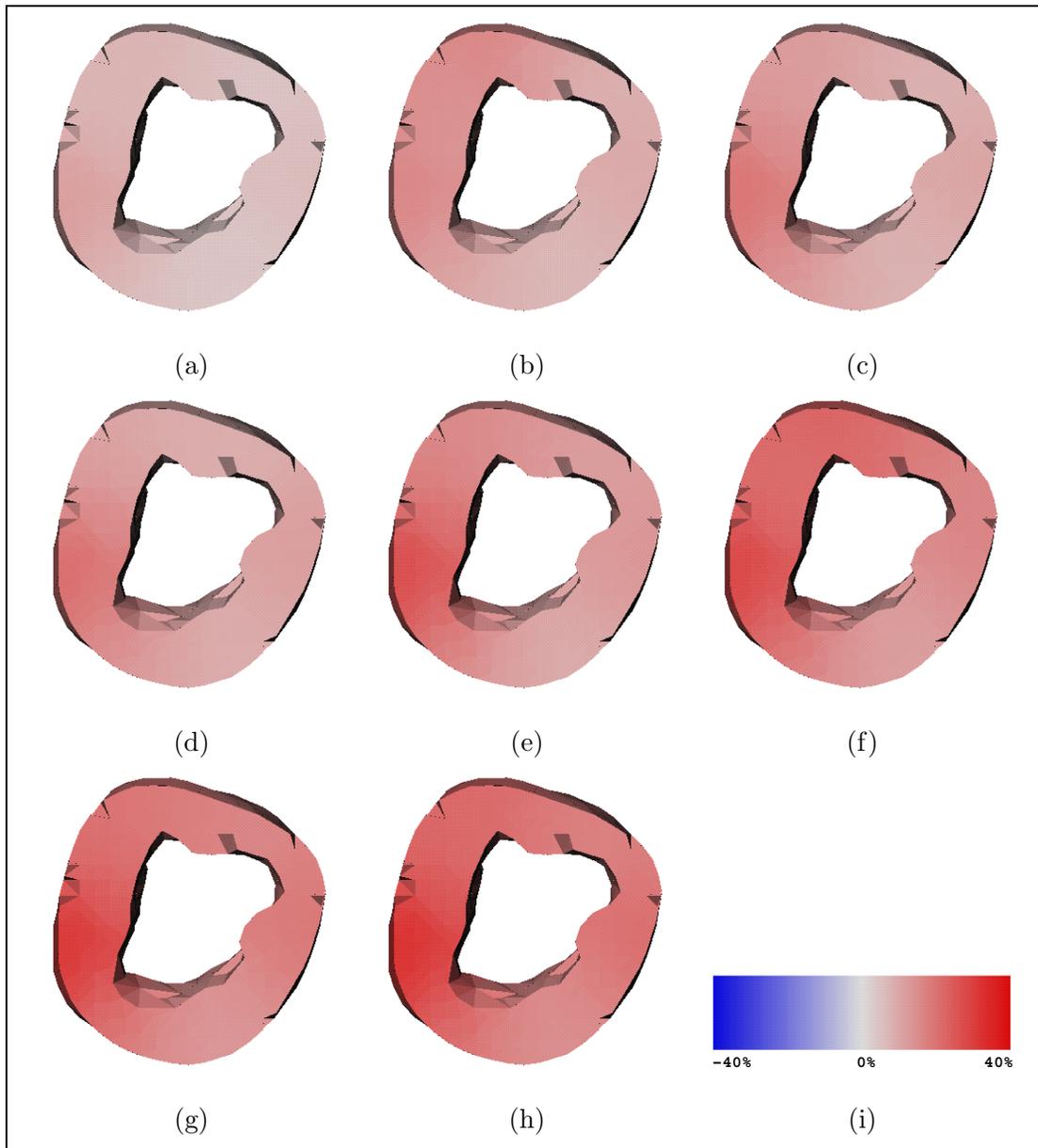
Figure 7: Temporal maps of the maximum principal strain (ED-ES) from phase contrast MR images. Note that at ES, the anterior septal region has the highest average maximum principal strain, which coincides with the injury region observed from post mortem TTC staining. (a)-(h): the eight maximum principal strain maps from ED to ES; (i): color scale.